ISSN 0036-0236, Russian Journal of Inorganic Chemistry, 2016, Vol. 61, No. 9, pp. 1061–1069. © Pleiades Publishing, Ltd., 2016.
Original Russian Text © T.L. Egorova, M.V. Kalinina, E.P. Simonenko, N.P. Simonenko, O.A. Shilova, V.G. Sevastyanov, N.T. Kuznetsov, 2016, published in Zhurnal Neorganicheskoi Khimii, 2016, Vol. 61, No. 9, pp. 1115–1124.

SYNTHESIS AND PROPERTIES OF INORGANIC COMPOUNDS

Liquid-Phase Synthesis and Physicochemical Properties of Xerogels, Nanopowders and Thin Films of the CeO_2–Y_2O_3 System

T. L. Egorova[a], M. V. Kalinina[a], E. P. Simonenko[b], N. P. Simonenko[b], O. A. Shilova[a, c], V. G. Sevastyanov[b], and N. T. Kuznetsov[b]

[a] *Grebenshchikov Institute of Silicate Chemistry, Russian Academy of Sciences, St. Petersburg, Russia*
[b] *Kurnakov Institute of General and Inorganic Chemistry, Russian Academy of Sciences, Leninskii pr. 31, Moscow 119991 Russia*
[c] *St. Petersburg State Electrotechnical University (LETI), St. Petersburg, Russia*
e-mail: egorova.offver@gmail.com

Received February 16, 2016

Abstract—Low-agglomerated xerogels, ultrafine oxide powders with particle sizes of 12–20 nm, and uniform thin films with particle sizes of 8–14 nm are prepared in the CeO_2–Y_2O_3 system using liquid-phase low-temperature methods, namely via coprecipitation of hydroxides and cocrystallization of salts, sol–gel technology. A comparative characterization of the prepared xerogels and nanopowders is performed using a set of physicochemical analytical methods. A dependence of phase composition, microstructure, and particle size on synthetic parameters is elucidated.

DOI: 10.1134/S0036023616090047

In the first decades of the XXI century, it becomes obvious that the inertial development of existing technologies in the energy sector to a greater extent is exhausted, and there is need to look for innovative ways to transform the energy sector [1–3]. In this context, hydrogen power engineering programs are of the highest priority in today's energy strategy, one of the promising directions of which is the development of fuel cells (FCs) [1, 4, 5]. The economic efficiency of power plants based on fuel cells is almost twice higher than that of conventional power plants; their figures of merits can amount to 70–85% taking into account heat recovery, and hazardous emissions are nearly 100 times as low due to the absence of direct chemical contact between the fuel and the oxidant [6, 7].

The high operating temperatures of solid oxide fuel cells (SOFCs) lead to their high costs and pose the problem of compatibility of electrolyte and electrode materials. Therefore, reducing their operating temperatures and developing medium-temperature SOFCs is an important task of materials science at the global level [8–10].

Ceria-based ceramic nanomaterials were found to be an alternative to YSZ (ZrO_2 + 8 mol % Y_2O_3), which was the most popular electrolyte material. Ceria-based electrolyte materials have a number of advantages: they have higher conductivity values at the same dopant concentrations; ceria has a fluorite-like cubic structure, so its base solid solutions can be studied even at very low dopant concentrations where structural defects obey the mass-action law [11]. The highest electrical conductivity for CeO_2 and its base solid solutions is attained when dopant ions have similar ionic radii but lower oxidation numbers (Y^{3+}, Gd^{3+}, Sm^{3+}, and other [12, 13]). That is why a lot of interest of researchers in recent years focuses just on the CeO_2–Y_2O_3 system; a characteristic feature of this system is the high yttrium solubility in the ceria crystal lattice (up to 40%), which is due to close values of yttrium and cerium ionic radii ($r_{Y^{3+}}$ = 0.090 Å; $r_{Ce^{4+}}$ = 0.092 Å [14–16]). This heterovalent ion substitution in the cationic sublattice of the CeO_2 cubic lattice suggests the generation of oxygen vacancies and the attendant appearance of oxygen ion conduction, which is the key criterion for the suitability of an electrolyte material for SOFC manufacture.

Of special interest are thin-film electrolyte materials, as well as FCs and fuel batteries [17, 18], in view of the following advantages of planar constructs: (1) high packing densities of elements in the cell (battery), which makes achievable higher working surface to volume ratios; (2) the ability to improve the efficiency and increase the performance resource of a SOFC by reducing the impedance of the cell through reducing the thickness of cell (battery) components.

The basic processes for producing oxide nanopowders and materials based on rare-earth elements are various variants of chemical methods, namely: coprecipitation of hydroxides [19], cocrystallization of salts [20], sol–gel process [21–24], and other technologies, so the role of controlled chemical synthesis becomes decisive in generating and modifying the

properties of materials. It is the stage of forming xerogels and powders on their base that provides for the acquisition by ceramic materials of their dimensional, phase, and structural characteristics and thereby chemical, physical, and mechanical properties.

Thus, our goal in this study was to make technological foundations for tailored liquid-phase synthesis based on the coprecipitation of oxides and cocrystallization of salts, sol–gel technology for preparing xerogels, nanosized oxide powders, and thin films of tailored chemical compositions in the CeO_2–Y_2O_3 system; one more our goal was a comparison study of the thus-prepared xerogels, nanosized powders, and thin films by a set of physicochemical methods.

EXPERIMENTAL

The reagents used were: $Ce(NO_3)_3 \cdot 6H_2O$ (chemically pure grade), $Y(NO_3)_3 \cdot 6H_2O$ (chemically pure grade), $NH_3 \cdot H_2O$ (specialty grade), $C_5H_8O_2$ (pure grade) and $^iC_5H_{11}OH$ (pure for analysis grade).

Potentiometric titration of solutions to determine the pH range for hydroxide deposition was performed with a 150 M ion meter.

X-ray powder diffraction experiment for determining the phase compositions of powders was performed on a Bruker D8-Advance diffractometer. Patterns were recorded in the range 5°–80° 2θ at room temperature under air. The ICDD-2006 File was used to interpret the patterns. Mean crystallize sizes were calculated by the Debye–Scherrer relationship: $d = 0.9\ \lambda/(\beta\cos\theta)$, where d is mean crystallite size, λ is CuK_α radiation length, and β is diffraction peak half-width [25].

The thermolysis of xerogels under air and argon was studied using an SDT Q-600 TG/DSC/DTA analyzer.

Powders and films were heat-treated in an AB Utenos Elektrotechnika programmable muffle furnace at temperatures in the range 25–1000°C.

The IR transmittance spectra of powders were recorded as Nujol mulls in KBr glasses on an Infralum FT-08 FTIR spectrometer.

A scanning electron microscopy experiment to study the surface morphology of prepared thin films was performed on a Carl Zeiss NVision 40 three-beam workstation.

Atomic-force microscopy to determine the surface relief and morphology of thin films was carried out using a Solver Pro-M probe microscope (NT-MDT).

The adherence of films was measured by a notch test using an Elcometer 107 adhesion meter.

RESULTS AND DISCUSSION

Preparation of $(CeO_2)_{0.80}(Y_2O_3)_{0.20}$, $(CeO_2)_{0.85}(Y_2O_3)_{0.15}$, and $(CeO_2)_{0.90}(Y_2O_3)_{0.10}$ Nanocrystalline Powders

Hydroxide coprecipitation route. We chose the hydroxide coprecipitation route to prepare samples with varied oxide concentration ratios in the CeO_2–Y_2O_3 system. Dilute solutions (~0.1 mol/L) were prepared from $Y(NO_3)_3 \cdot 6H_2O$ and $Ce(NO_3)_3 \cdot 6H_2O$ [19]. Dilute solutions are more suitable for precipitation, as providing for a higher dispersion of precipitation products. Preliminarily, pH-titration showed that hydroxides were precipitated from salt solutions by aqueous ammonia ($NH_3 \cdot H_2O$) in different pH ranges (table).

In view of the precipitation pH for each hydroxide, pH in the reactor was maintained in the range 10.1–10.3; $NH_3 \cdot H_2O$ concentration was ~1 mol/L. The precipitation was carried out at a minimal rate (v_{pr} = 0.02 cm^3/s) with careful stirring.

In order to deagglomerate the coprecipitated products in the CeO_2–Y_2O_3 system, the gels were kept frozen at –25°C for 24 h to deeply dehydrate them and preserve the high dispersion of the coprecipitated powders. When a gel is frozen, it cures as rapidly as possible, along with eliminating adsorbate and crystal water, so the solid retains the high chemical homogeneity intrinsic to the coprecipitated product.

Salt cocrystallization route. A nanosized oxide in the CeO_2–Y_2O_3 system was also prepared by the salt cocrystallization route, which promotes interactions of chemical components at the levels of ions and molecules. This route, thanks to high degrees of homogenization, minimizes the role of high-temperature diffusion, at the same time being rather facile and not requiring intricate hardware. Cerium nitrate and yttrium nitrate were used to prepare oxides with various metal ratios in the CeO_2–Y_2O_3 system; their solutions were prepared to have concentration of ~0.5 mol/L. These solutions were mixed to fulfill the desired metal stoichiometry, and mixed solutions were concentrated

Precipitation pH for yttrium and cerium hydroxides

Initial reagent (salt)	Aqueous salt solution, mol/L	Precipitating hydroxide	Deposition pH range
$Ce(NO_3)_3 \cdot 6H_2O$	0.1	$Ce(OH)_3$	8.3–9.8
$Y(NO_3)_3 \cdot 6H_2O$	0.1	$Y(OH)_3$	6.8–7.5

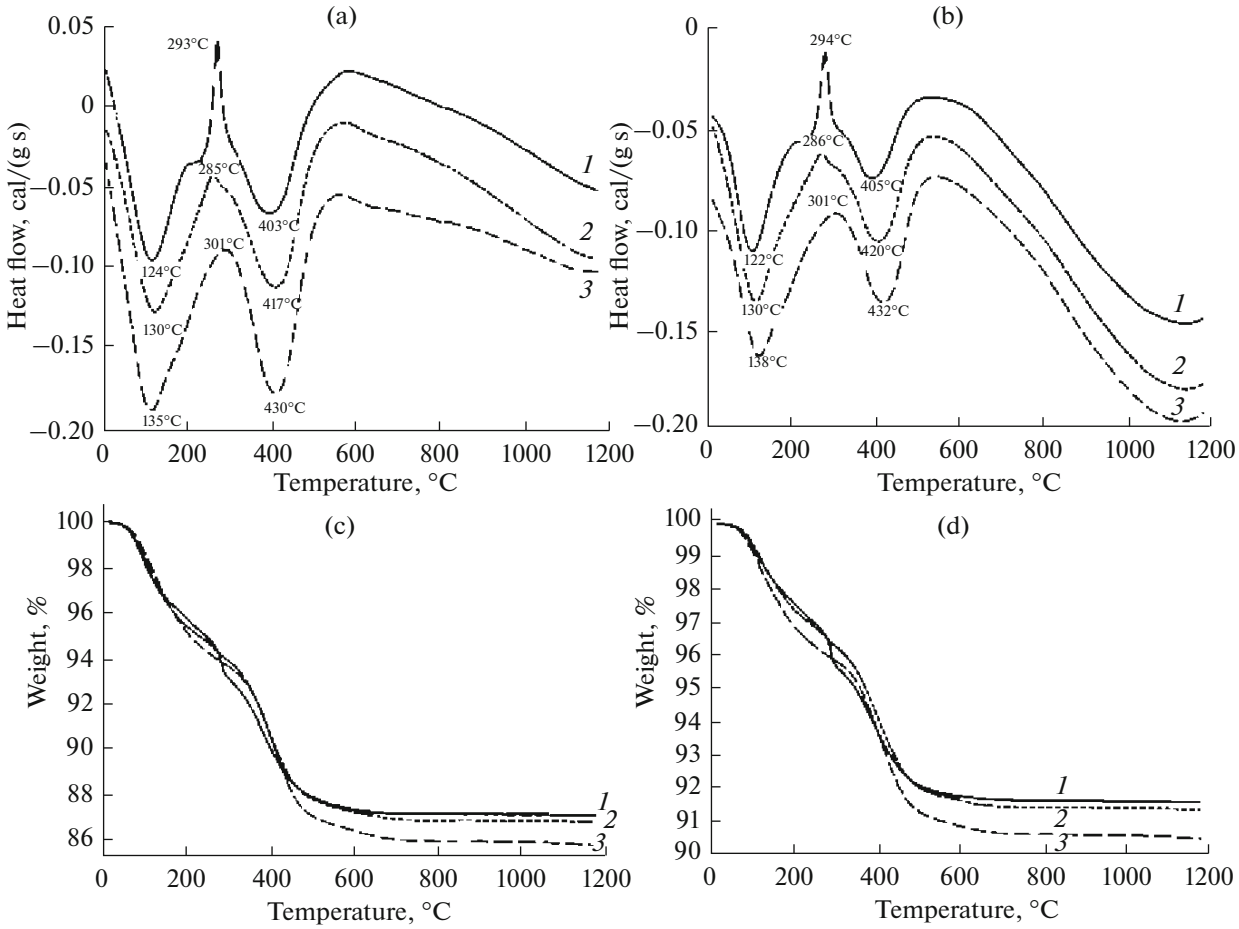

Fig. 1. (a, b) DSC curves (a) in flowing air and (b) in argon and (c, d) TG curves (c) in flowing air and (d) in argon for (*1*) $(CeO_2)_{0.9}(Y_2O_3)_{0.1}$, (*2*) $(CeO_2)_{0.85}(Y_2O_3)_{0.15}$, and (*3*) $(CeO_2)_{0.80}(Y_2O_3)_{0.20}$ xerogels.

on a water bath for 5 h until supersaturation was attained [20].

The degree of supersaturation increases as a solution becomes progressively concentrated, favoring the crystallization onset: the nucleation of a new phase in the form of crystallization centers, which gradually transform to fine crystals that are piled up on the solution surface.

The supersaturated solution was cooled at 3–5°C to enhance the adsorption of the newly crystallizing material on the surfaces of crystals that were formed upon the concentration of mixed salt solutions. Crystallization should not be too fast, as if so, crystals would be grown rapidly and could capture three-dimensional inclusions of the medium, so the homogeneity of the product will be spoiled.

Preparation of $(CeO_2)_{0.80}(Y_2O_3)_{0.20}$, $(CeO_2)_{0.85}(Y_2O_3)_{0.15}$, and $(CeO_2)_{0.90}(Y_2O_3)_{0.10}$ Thin Films

Acetylacetonates $[Ce(C_5H_7O_2)_3]$ and $[Y(C_5H_7O_2)_3]$ were prepared from the respective metal nitrates by adding acetylacetone and aqueous ammonia to aqueous nitrate solutions. Hydrolytically active heteroligand precursors $[M(C_5H_7O_2)_{3-x}(C_5H_{11}O^i)_x]$ (where $M = Ce^{3+}$ and Y^{3+}) were prepared by heat-treating the thus-prepared cerium and yttrium β-diketonates in isoamyl alcohol to cause a partial destructive replacement of chelating ligands by alkoxy moieties. Next, thin films of the solutions with the required metal ratio were applied to the surface of polished single-crystalline silicon and polycrystalline sapphire substrates by means of dip coating. After the hydrolysis of complexes by atmospheric moisture was over and xerogel coatings were formed, heat treatment was carried out in air for oxides to crystallize at 500–800°C (1-h exposure).

Characterization of $(CeO_2)_{0.80}(Y_2O_3)_{0.20}$, $(CeO_2)_{0.85}(Y_2O_3)_{0.15}$, and $(CeO_2)_{0.90}(Y_2O_3)_{0.10}$ Xerogels and Nanopowders

The thermolysis of $(CeO_2)_{0.80}(Y_2O_3)_{0.20}$, $(CeO_2)_{0.85}(Y_2O_3)_{0.15}$, and $(CeO_2)_{0.90}(Y_2O_3)_{0.10}$ xerogels prepared by the hydroxide coprecipitation route was studied using simultaneous TG/DSC thermal analysis

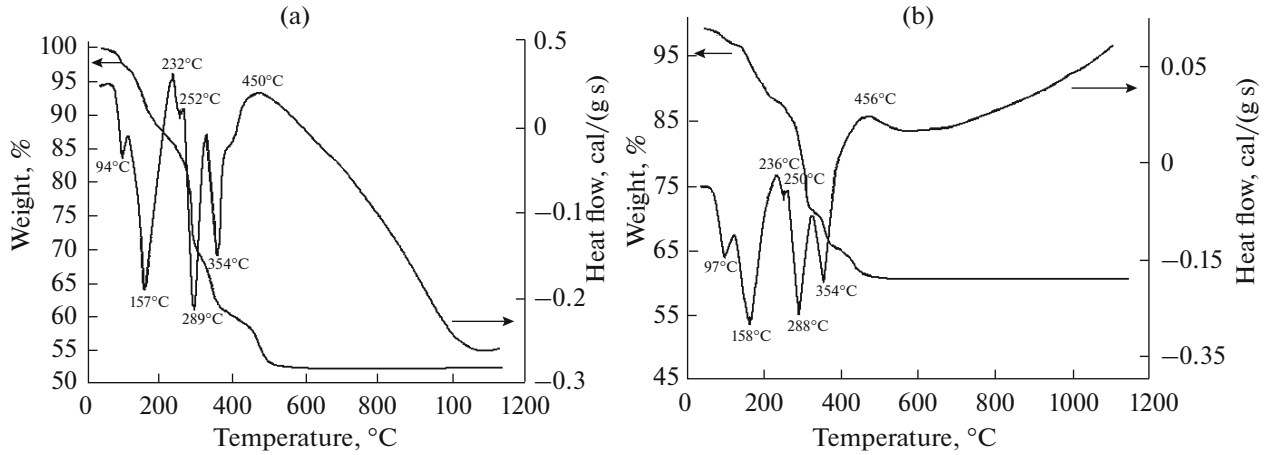

Fig. 2. DSC and TG curves (a) in flowing air and (b) in argon for a $(CeO_2)_{0.80}(Y_2O_3)_{0.20}$ xerogel prepared by cocrystallization.

in flowing air and argon (Fig. 1). Figure 1 shows that a change in gas flow affects the thermal behavior of powders less strongly than varying metal ratio does. All samples under heating typically show a stepped weight loss with attendant endotherms in the range 20–300°C (Δm is ~5–6% in flowing air and ~3–4% in flowing argon) and 300–550°C (Δm ~ 6–7% in flowing air and ~4–5% in flowing argon), associated with the dehydration and degradation of cerium and yttrium complex hydroxides. The intensities of these endotherms and the values of relevant weight loss steps (as well as the overall weight loss of the sample upon heating to 1200°C) in flowing air are higher than in flowing inert gas, and increase as the yttrium content increases.

An exotherm also appears in the range 200–300°C on DSC curves for $(CeO_2)_{0.90}(Y_2O_3)_{0.10}$ and $(CeO_2)_{0.85}(Y_2O_3)_{0.15}$ xerogels; its intensity, as the attendant weight loss, too, increases as the yttrium content decreases. This exotherm presumably arises from the oxidation—reduction process typical of cerium oxide ($Ce^{3+} \rightarrow Ce^{4+}$) in air medium; in argon, the exotherm also appears, but is less prominent. The cubic solid solution that exists in the CeO_2–Y_2O_3 system crystallizes in the range 300–550°C. However, there is no exotherm due to the crystallization of cubic solid solution. The nonappearance of the relevant exotherm is due to the smooth and continuous, rather than explosion-like, character of crystallization and its concurrency with the degradation of hydroxides. An inert gas atmosphere during thermal analysis was shown to reduce the intensity of this process: the heat and weight loss decrease (Δm for $(CeO_2)_{0.90}(Y_2O_3)_{0.10}$ is ~2% in flowing air and ~1% in flowing argon). The peak temperature of this exotherm was found to shift by 8°C toward low temperatures from 293°C for $(CeO_2)_{0.90}(Y_2O_3)_{0.10}$ to 285°C for $(CeO_2)_{0.85}(Y_2O_3)_{0.15}$ (in response to increasing yttrium content) in an oxygen-containing atmosphere and, respectively, from 294 to 286°C in flowing argon. Figure 1 makes it clear that all the above-described processes have their heats increasing as yttrium concentration rises. This trend arises from the fact that the degradation of yttrium hydroxide, which is a constituent of the mixed hydroxide, is a complex process, occurs in steps, and is accompanied by several endotherms.

A comparison analysis of thermolysis processes under air and under argon shows a similarity of the two; under the inert atmosphere, however, the thermal features are weaker. Thus, the results of simultaneous TG/DSC analysis of prepared xerogels clearly show the dependence of their thermal behavior on the metal ratio and gas atmosphere composition.

For the crystal hydrates prepared by the cocrystallization of cerium and yttrium nitrates, thermolysis in flowing air and in flowing argon was also studied by simultaneous TG/DSC analysis (Fig. 2). From the thermoanalytical curves for the powder that corresponds to the target composition $(CeO_2)_{0.80}(Y_2O_3)_{0.20}$, one can infer that a rise in temperature gives rise to a complex, six-step weight loss process, where five steps are accompanied with endotherms with peaks at 94, 157, 252, 289, and 354°C in flowing air and at 97, 158, 250, 288, and 354°C in flowing argon. These steps are associated with the dehydration and degradation of cerium and yttrium nitrates. The peaks of the first two low-temperature endotherms shift toward higher temperatures when the powder is heated under the inert atmosphere while the next two peaks, in contrast, shift toward lower temperatures. The peak temperature of the fifth weight loss peak is independent of the flowing gas composition. In the range 400–450°C, a low-intensity exotherm is observed (with weight loss of ~8% in flowing air and ~5% in flowing argon), apparently corresponding to the crystallization of the ceria-base cubic solid solution. The TG curves imply that the powder weight stabilizes at temperatures of about 500°C and the overall value Δm upon heating to

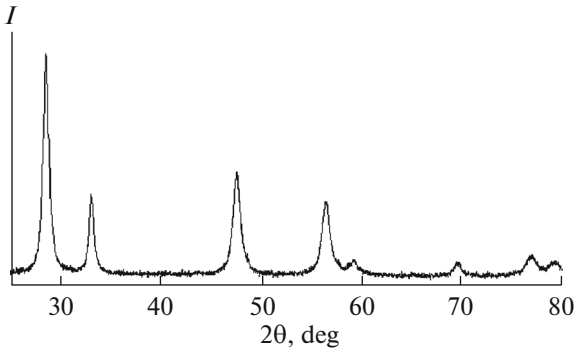

Fig. 3. X-ray diffraction pattern of a $(CeO_2)_{0.80}(Y_2O_3)_{0.20}$ precursor powder prepared by coprecipitation at 600°C.

1200°C is ~47% in flowing air and ~40% in flowing argon.

A comparison analysis of the thermolysis of xerogels prepared by the hydroxide coprecipitation route and the salt cocrystallization route, shows that the weight loss due to dehydration in far smaller in the former. This result is due to the following. Coprecipitation, a finer chemical synthesis, involves elements of cryotechnology, namely freezing of precipitated hydroxides at −25°C to remove adsorbate water and most crystal water. Treatment at −25°C favors weakening of intermolecular interactions between particles in hydroxides and thereby increases the dispersion of the precipitated product and activates dehydration. As probed by X-ray powder diffraction, the ultrafine nanopowders prepared by coprecipitation at 600°C, have fluorite-type cubic structure (Fig. 3) with the unit cell parameter $a = 5.4$ Å and mean crystallite size of ~12 nm, and nanopowders prepared by cocrystallization have the same structure but a larger mean crystallite size (~20 nm).

Thus, the coprecipitation route yields finer $(CeO_2)_{0.80}(Y_2O_3)_{0.20}$, $(CeO_2)_{0.85}(Y_2O_3)_{0.15}$, and $(CeO_2)_{0.90}(Y_2O_3)_{0.10}$ powders than the cocrystallization route does.

Fourier-transform IR spectroscopy was used to study the xerogels and nanopowders (Fig. 4) of composition $(CeO_2)_{0.80–0.90}(Y_2O_3)_{0.20–0.10}$ prepared by the two liquid-phase synthesis routes.

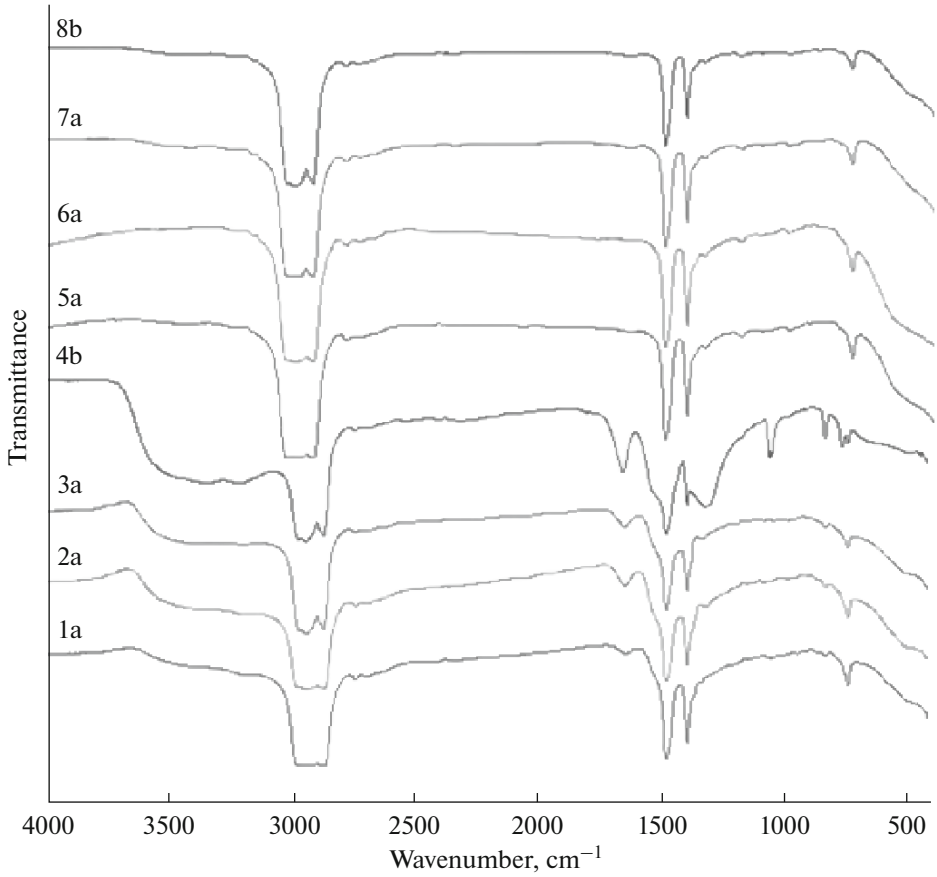

Fig. 4. IR transmittance spectra for xerogels **1**–**4** and nanopowders **5**–**8** prepared by (a) coprecipitation and (b) cocrystallization: (1a) $(CeO_2)_{0.90}(Y_2O_3)_{0.10}$, (2a) $(CeO_2)_{0.85}(Y_2O_3)_{0.15}$, (3a) $(CeO_2)_{0.80}(Y_2O_3)_{0.20}$, (4b) $(CeO_2)_{0.80}(Y_2O_3)_{0.20}$, (5a) $(CeO_2)_{0.90}(Y_2O_3)_{0.10}$, (6a) $(CeO_2)_{0.85}(Y_2O_3)_{0.15}$, (7a) $(CeO_2)_{0.80}(Y_2O_3)_{0.20}$, and (8b) $(CeO_2)_{0.80}(Y_2O_3)_{0.20}$.

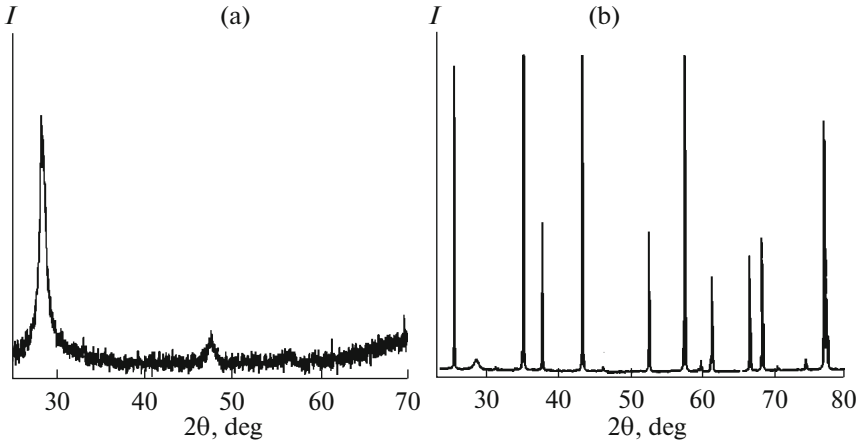

Fig. 5. X-ray diffraction patterns of $(CeO_2)_{0.8}(Y_2O_3)_{0.2}$ films prepared at 800°C for 1 h (a) on silicon, $d = 13.4$ nm; and (b) on sapphire, $d = 14$ nm.

The absorption bands in the range 3000–3750 cm^{-1} (the stretching vibrations of OH groups) and those in the range 1600–1630 cm^{-1} (the bending vibrations of HOH) signify the presence of crystal water in the xerogels. The amount of crystal water in samples **1**–**3**, which were prepared by coprecipitation, is far lower than in sample **4**, which was prepared by the cocrystallization route. This finding agrees with the results of thermal analysis and supports the efficiency of using cryotechnology elements in the coprecipitation route. In the range 400–500 cm^{-1}, there is a weak vibration mode Ce(Y)–O. The absorption bands with peaks at 1316, 1041, and 815 cm^{-1} in sample **4** relate to the vibrations of nitrate ions in cerium and yttrium nitrates. After heat treatment at 600°C for 1 h, the IR spectra of samples **5**–**8** feature no absorption bands typical of crystal water and nitrate ions; this means that these species were removed and a metastable crystal structure of solid solutions was formed in the CeO_2–Y_2O_3 system.

Characterization of $(CeO_2)_{0.80}(Y_2O_3)_{0.20}$, $(CeO_2)_{0.85}(Y_2O_3)_{0.15}$, and $(CeO_2)_{0.90}(Y_2O_3)_{0.10}$ Thin Films

Films prepared by the above-described routes of sol–gel technology were characterized by X-ray powder diffraction. Figure 5 shows exemplary X-ray diffraction patterns for $(CeO_2)_{0.80}(Y_2O_3)_{0.20}$ thin films on polished single-crystalline silicon and polycrystalline sapphire substrates. One can see from this figure that the substrate material has no effect on the crystal structure of films. Fluorite cubic structure is obtained in both cases; the crystallite size is ~14 nm (when crystallized at 800°C). One can also see from Fig. 5 that the reflections from the Al_2O_3 substrate structure are far stronger than the characteristic reflections from the films, proving their thin-film structure. When the synthesis temperature increases from 500 to 800°C, the mean crystallite size in the thin films of compositions studied increases in the range 8–14 nm.

The microstructure of $(CeO_2)_{0.80–0.90}(Y_2O_3)_{0.20–0.10}$ films prepared by sol–gel technology on polished corundum and silicon substrates and then annealed at 500–800°C, was studied using scanning electron microscopy.

Those nanostructured films were found to refer to maximal adhesion classes of the ISO (0) and ASTM (5B) international standards.

Highly disperse uniform films, <100 nm thick, were prepared with fine-crystalline cellular microstructure (Fig. 6) and particle sizes of 8–14 nm. One can see from Fig. 6 that, as the annealing temperature of films on the substrate increases, the porosity of the films increases, too, and film surface morphology acquires the most well-defined cellular microstructure. Figure 7 shows micrographs of thin films of various compositions prepared at 600°C. One can see from this figure that increasing yttrium concentrations influence the morphology and surface structuring.

Film morphology was also studied by scanning probe microscopy (Fig. 8). As one can see from micrographs in Fig. 8, coatings of various compositions crystallized at 800°C, are nanostructured and follow the relief of silicon substrates, and this proves their good adherence to the substrates and thin-film structure. The results show that the films are continuous; the maximal height difference across a 25 μm^2 surface area does not exceed 30 nm.

Fulfilling this study, we have developed technological bases for targeted liquid-phase synthesis, through coprecipitation of hydroxides and cocrystallization of salts, sol–gel technology, for preparing low-agglomerated xerogels, ultrafine powders, and thin films of tailored compositions in the CeO_2–Y_2O_3 system, which are the base for design of SOFC electrolyte materials. A comparison analysis of the thermolysis of xerogels

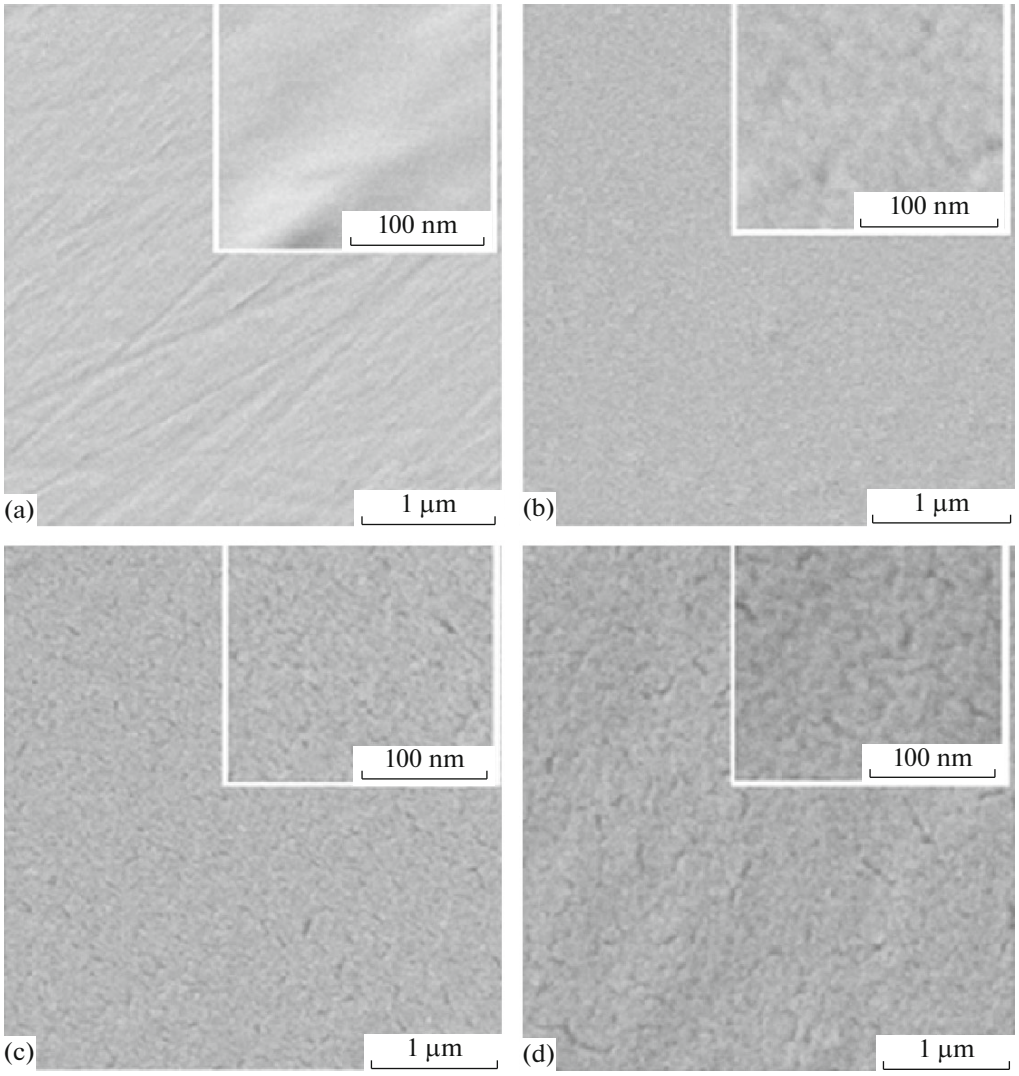

Fig. 6. Microstructures of $(CeO_2)_{0.90}(Y_2O_3)_{0.10}$ films on polished single-crystalline silicon substrates prepared by heat treatment for 1 h at various temperatures: (a) 500, (b) 600, (c) 700, and (d) 800°C.

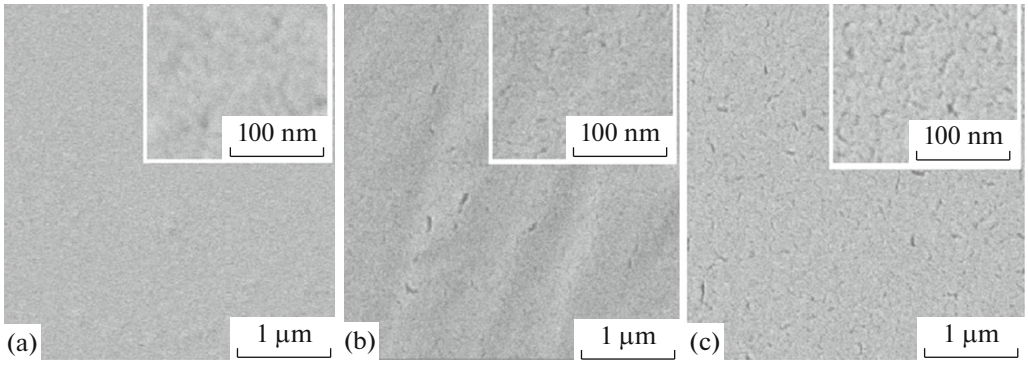

Fig. 7. Microstructures of (a) $(CeO_2)_{0.90}(Y_2O_3)_{0.10}$, (b) $(CeO_2)_{0.85}(Y_2O_3)_{0.15}$, and (c) $(CeO_2)_{0.80}(Y_2O_3)_{0.20}$ films on polished single-crystalline silicon substrates calcined at 600°C.

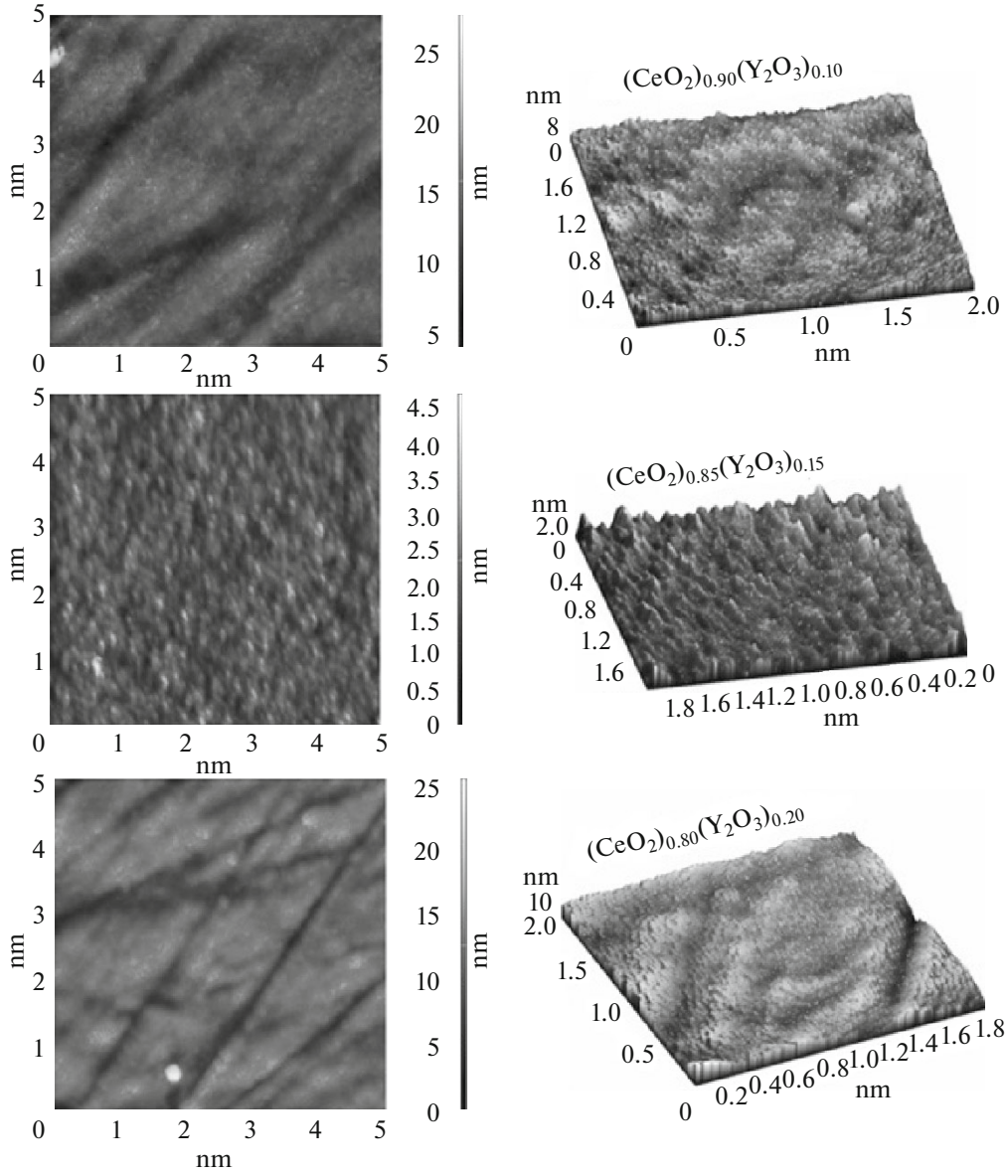

Fig. 8. Morphology of $(CeO_2)_{0.80–0.90}(Y_2O_3)_{0.20–0.10}$ films crystallized at 800°C (as probed by scanning probe microscopy).

prepared by two routes (hydroxide coprecipitation and salt cocrystallization) showed that the weight losses upon dehydration were far smaller in the coprecipitation route, which is the finest chemical method, due to the use of cryotechnology. These results were supported by IR spectroscopic characterization of CeO_2–Y_2O_3 xerogels and nanopowders. The nanopowders prepared by coprecipitation and then annealed 600°C were shown to have fluorite-type cubic crystal structure with the unit cell parameter a = 5.4 Å and the mean crystallite size of ~12 nm; the nanopowders prepared by cocrystallization had the same structure but a larger mean crystallite size (~20 nm). Thus, the prepared xerogels and nanosized powders in their physicochemical properties are candidates for use in design of nanoceramic electrolyte materials for medium-temperature solid oxide fuel cells.

The CeO_2–Y_2O_3 thin films prepared by sol–gel technology using heteroligand precursors with the tailored coordination sphere compositions, were also characterized by a set of physicochemical methods. Crystallized oxide films had fluorite cubic structure; mean crystallite sizes were 8–14 nm (depending on the synthesis temperature). We showed that this strategy yields, at low temperatures, thin nanostructured oxide films of complex composition on various substrates with continuous microstructure and the maximal adhesion classes according to ISO (0) and ASTM (5B) international standards in the absence of chemi-

cal interaction. The prepared films less than 100 nm thick have fine-grained cellular microstructure.

We have shown that our technology of forming thin oxide films in the CeO_2–Y_2O_3 system on various types of substrates using hydrolytically active heteroligand complexes $[M(C_5H_7O_2)_{3-x}(C_5H_{11}O^i)_x]$ ($M = Ce^{3+}$ and Y^{3+}) with the tailored reactivity will be suitable for preparing advanced electrolyte materials for medium-temperature planar SOFCs with improved efficiency and increased performance resources.

ACKNOWLEDGMENTS

This study was supported by the Russian Foundation for Basic Research (project mol_nr No. 15-33-51237).

REFERENCES

1. V. G. Rodionov, *Power Engineering: Current Topics and Potentials* (ENAS, Moscow, 2010) [in Russian].
2. S. A. Grigor'ev, V. I. Kostin, and A. S. Grigor'ev, Eur. J. Tech. Des. **1**, 28 (2013).
3. A. S. Lipilin, Elektrokhim. En. **7** (2), 61 (2007).
4. S. I. Kozlov, *Hydrogen Power Engineering: State of Art, Topics, Prospects* (Gazprom VNIIGAZ, Moscow, 2009) [in Russian].
5. A. S. Nesaraj, J. Sci. Ind. Res. **69**, 169 (2010).
6. A. K. Ivanov-Shits and I. V. Murin, Ionics of Solids, (SPbGU, St. Petersburg, 1000), Vol. 2 [in Russian].
7. M. Kuhn and T. W. Napporn, Energies **3**, 57 (2010).
8. H. A. Taroco, J. A. F. Santos, R. Z. Domingues, and T. Matencio, *Advances in Ceramics: Synthesis and Characterization, Processing and Specific Applications*, Ed. by C. Sikalidis (2011). ISBN: 978-953-307-505-1. InTech21
9. P. Holtappels, U. Vogt, and T. Graule, Adv. Eng. Mater. **7**, 292 (2005).
10. A. Tarancon, Energies **2**, 1130 (2009).
11. T. Mori, J. Drennan, D. R. Ou, et al., Nukleonika **51** (Suppl. 1), 11 (2006).
12. Y. P. Fu, S. H. Chen, and J. J. Huang, Int. J. Hydrogen En. **35**, 745 (2010).
13. N. Cioatera, V. Parvulescu, A. Rolle, et al., Ceram. Int. **38**, 5461 (2012).
14. G. V. Samsonov, *Physicochemical Properties of Oxides. Handbook* (Metallurgiya, Moscow, 1978) [in Russian].
15. T. Mori, J. Drennan, Y. Wang, et al., Sci. Technol. Adv. Mater. **4**, 213 (2003).
16. Y. Goto, K. Takahashi, T. Omataet, et al., J. Phys.: Conf. Ser. **165**, 1 (2009).
17. V. V. Ivanov, A. S. Lipilin, A. V. Spirin, et al., Altern. En. Ecol. **46** (2), 75 (2007).
18. C. Tian and S. W. Chan, J. Am. Ceram. Soc. **85**, 2222 (2002).
19. M. V. Kalinina, L. V. Morozova, I. I. Khlamov, et al., Glass Phys. Chem. **40**, 578 (2014).
20. A. S. Kovalenko, O. A. Shilova, L. V. Morozova, et al., Glass Phys. Chem. **40**, 106 (2014).
21. M. V. Kalinina, L. V. Morozova, T. L. Egorova, et al., Glass Phys. Chem. **41**, 431 (2015).
22. N. P. Simonenko, E. P. Simonenko, V. G. Sevastyanov, and N. T. Kuznetsov, Russ. J. Inorg. Chem. **60**, 795 (2015). doi 10.1134/S0036023615070153.
23. E. P. Simonenko, N. P. Simonenko, V. G. Sevastyanov, and N. T. Kuznetsov, Russ. J. Inorg. Chem. **57**, 1521 (2012). doi 10.1134/S0036023615070153.
24. M. V. Kalinina and P. A. Tikhonov, et al., Glass Phys. Chem. **40**, 629 (2014).
25. P. Duran, M. Villegas, and F. Capel, J. Eur. Ceram. Soc. **16**, 945 (1996).

Translated by O. Fedorova